Investigation on the effect of exposure time on scintillator afterglow for ultra-fast tomography acquisition

Investigation on the effect of Exposure Time on Scintillator Afterglow for Ultra-Fast Tomography Acquisition

Karim Zarei Zefreh [a,*], Federica Marone Welford[b], Jan Sijbers [a]

[a] *imec-VisionLab, University of Antwerp, Wilrijke, Belgium*

[b] *X-ray Tomography Group, Swiss Light Source, Villigen, Switzerland*

E-mail: karim.zareizefreh@uantwerpen.be

ABSTRACT: Thanks to the ultra-fast endstation of the TOMCAT beamline, it is possible to do a tomographic scan with a sub-second temporal resolution which allows following dynamic processes in 4D (3D space + time). This ultra- high-rate tomography acquisition, exploiting the distinctive peculiarities of synchrotron radiation, provides nondestructive investigation of many dynamic processes which were not possible in the past. For example a continuous tensile test has been conducted recently in-situ for the first time with a frequency of 20 tomograms per second (20 Hz acquisition frequency). In the ultra-fast endstation a scintillator is used to convert X-ray to visible photons that can be detected by the camera. However, this conversion is not ideal and the scintillator response decays exponentially with afterglow. Afterglow can cause resolution degradation and artifacts (such as ring and band) especially with high rotation speed. On the other hand, to achieve a higher scan speed, thicker scintillators are more common because they result in higher emission intensities that can compensate the short exposure time in fast scans. However, the resolution deteriorates as the scintillator's thickness increases and thicker scintillators show higher afterglow. Performing many ultra-fast scans at the TOMCAT beamline with different acquisition rate, we demonstrate how the exposure time effects on the projection data and reconstructed images. Using two different thicknesses of LAG scintillator we also investigate the afterglow artifacts for different acquisition rate and exposure time.

KEYWORDS: Exposure Time; Scintillator; Afterglow; Artifact; Ultra-fast Tomography.

Contents

1. Introduction

Thanks to the ultra-fast endstation of the TOMCAT beamline [1], it is possible to do a tomographic scan with a sub-second (up to 50ms) temporal resolution which allows following dynamic processes in 4D (3D space + time). This ultra- high-rate tomography acquisition, exploiting the distinctive peculiarities of synchrotron radiation, provides non-destructive investigation of many dynamic processes which were not possible in the past. For example a continuous tensile test has been conducted recently in-situ for the first time with a frequency of 20 tomograms per second (20 Hz acquisition frequency) [2]. Solid-state scintillation detectors are used at the TOMCAT ultra-fast endstation. Such detectors essentially consist of two main components: a scintillating medium and a visible light sensor (e.g. photodiode, CCD). The scintillator re-emits the absorbed energy deposited by incident ionizing radiation (e.g. X-rays) in the form of (scintillation) light. The chip sensor subsequently detects the scintillation light and converts it into an electric signal (current). The integrated current over a specified time is then, ideally, proportional to the total X-ray energy deposited in the scintillator over that time period. In practice, however, the excited states of the scintillator decay exponentially with certain characteristic time constants, which are dependent on the material and thickness of the scintillator as well as the conditions of excitation [3,4,5].

The short time constant components determine the primary speed of the detector while the afterglow refers to the remaining slower non-exponential components. If the primary speed is on the same order as the data acquisition rate, contamination from one measurement to the next will be present, mainly deteriorating the spatial resolution, distorting the reconstructed image and introducing an inhomogeneous noise pattern, especially for dynamical imaging [4,6]. The relative contribution of the afterglow to the overall signal is typically only a few percent [7]. While its impact on the spatial resolution is minimal, afterglow may lead to ring or band artifacts in the reconstructed images arising from the typical non-uniform afterglow characteristics of scintillator screens [3,8]. To minimize these artifacts, it is important to properly account for afterglow, prior to tomographic reconstruction particularly for ultra-fast scan [9].

The paper is organized as follows. An overview of the experimental setup is given in Section 2. In section 3, the explanation of the experiments and the results are presented. Finally, in Section 4, conclusions are drawn.

2. Experimental setup

At present, no standard procedure for evaluating detector image lag has been developed. That is, each detector manufacturer for X-ray CT or security systems evaluates the afterglow on the basis of their company standard system. Typical systems use a mechanical shutter or pulsed voltage control to turn on or off the X-ray source and measure the scintillator decay. To measure the X-ray-induced afterglow phenomenon, we performed our experiments with the standard setup of the TOMCAT beamline at Swiss Light Source (SLS). Moreover, the TOMCAT beamline provides a millisecond shutter (SLS 2004) to control the irradiation time of the samples with x-rays. The SLS 2004 millisecond shutter is a single-shot x-ray shutter system. It consists of a mechanical shutter and driver electronics, which can easily be interfaced to any control system. The SLS 2004 millisecond shutter can provide accurate irradiation times down to 2ms. The standard setup of the TOMCAT beamline is shown in Figure 1.

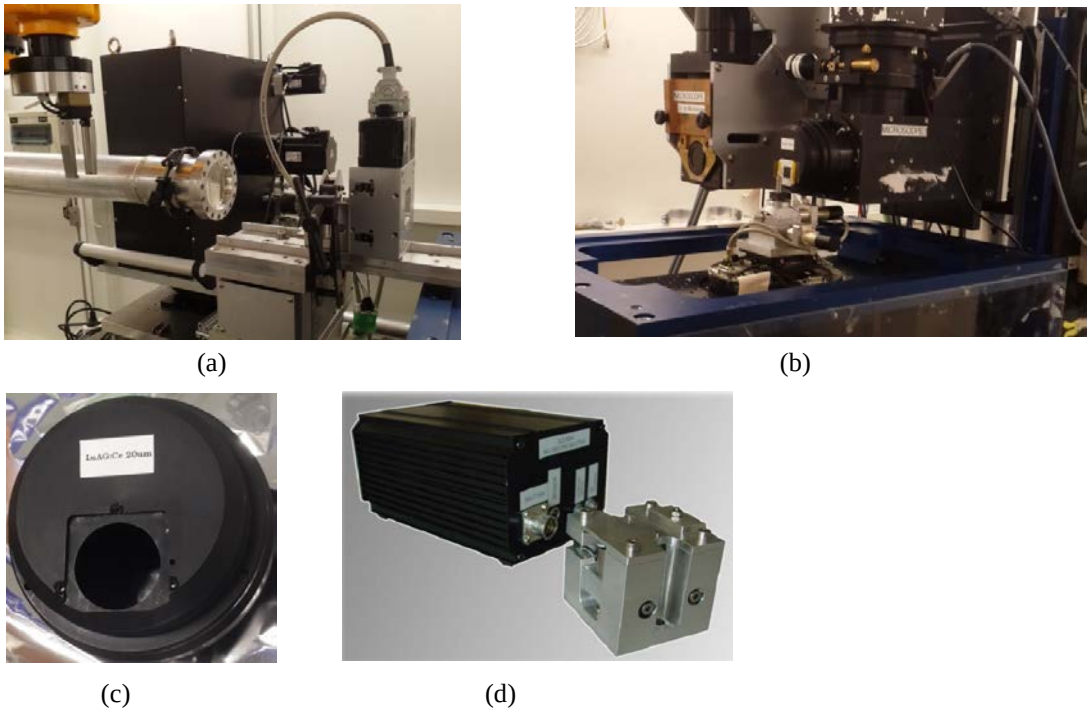

(a) (b)

(c) (d)

Figure 1: Experimental standard setup at the TOMCAT beamline. (a) The beamline vacuum fly tube and beam conditioning tower with the SLS 2004 Millisecond Shutter and a slit system. (b) Two different microscope optics with scintillators. (c) Close-up view of the mounting place for the scintillator. (d) SLS 2004 Millisecond Shutter and its control unit.

To investigate the effect of temporal resolution (scan speed) on the afterglow artifacts second part of the experiments were performed using the ultra-fast setup on a 2.9 T superbend as source with a critical energy at 11.9 keV. The phantom was placed at about 25 m downstream from the source. Filtered polychromatic X-rays (dumping 5 % of the total power) with a mean energy of 30 keV were incident on the sample attached to the tomography stage with three translational and one rotational degrees of freedom. The X-rays passing through the sample were converted to visible light by a LuAG:Ce converter and detected by an in-house developed 12 bit CMOS camera (giga-FROST) providing continuous acquisition up to 8GB/s. The camera was attached to the scintilator through a high numerical aperture microscope with continuous zoom option in

the range of 2×−4×in our case set to an effective pixel size of 4.4µm. In this setup the maximum rotation speed of the high-precision stage is 600 rpm and by that the limit of tomographic acquisition speed was 20 Hz. The TOMCAT ultra-fast setup is shown in Figure 2.

(a) (b) (c)

Figure 2: Ultra-fast setup at the TOMCAT ; (a) The beamline vacuum fly tube and beam conditioning tower. (b) 2-4x continuous magnification microscope: Elya Solutions. (c) Rotation stage and giga-FROST camera on top of the microscope.

3. Experiments

3.1 The effect of scintillator thickness on afterglow

To achieve a higher scan speed, thicker scintillators are more common because they result in higher emission intensities that can compensate the short exposure time in fast scans. However, the resolution deteriorates as the scintillator's thickness increases and thicker scintillators may show higher afterglow. To investigate the effect of scintillator thickness on the afterglow, we performed our experiments using different thicknesses (20um, 100um and 300um) of LAG:Ce scintillator. LuAG:Ce, Lutetium Aluminum Garnet doped with cerium (chemical formula $Lu_3Al_5O_{12}:Ce^{3+}$), is a relatively dense and fast scintillation material. LAG:Ce scintillators (from Crytur, Czech Republic [10]) are used typically at the TOMCAT beamline for absorption-based and phase contrast radiography and tomography. Table 1 shows the main characteristics of this scintillator. As it is shown in Figure 3, the maximum quantum efficiency of the camera (~50% at 535 nm) is well matched to the scintillator.

Table 1: LAG scintillator for X-ray imaging applications [10]

Name	Scintillator	Zeff	ρ(g/cm3)	Light yield(Ph/MeV)	λ (nm)
LAG	$Lu_3Al_5O_{12}:Ce^{3+}$	61	6.73	25	535

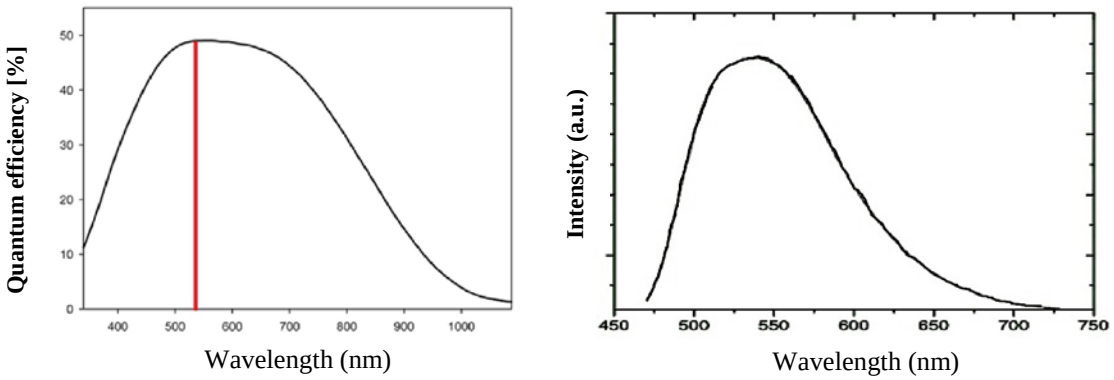

Figure 3: Quantum efficiency of the camera and fluorescence curve of the LAG scintillator.

In order to examine the effect of scintillator thickness on afterglow, we measured the scintillator decay following this protocol:
First 10 dark field images were acquired. These frames were used later to compensate for the detector offset.
Next, the millisecond shutter is opened and the scintillator is irradiated for a specific time (e.g. 200ms), controlled by a hardware trigger. The X-ray energy for this experiment was 18 keV.
After irradiation, we stopped the X-ray exposure by closing the shutter and read out the detector for 10 seconds. The normalized mean intensity of the frames that are acquired after closing the shutter represent the amount of afterglow.
Thicker scintillators result in higher emission intensities. Therefore, to compare the images for one scintillating material with different thicknesses, we should first normalize the data. To this end we used the conventional flat field correction (FFC) method [11]. The average of the first 10 images was used as the detector offset (dark image) and the mean of the images acquired during irradiation calculated as a flat image. As we see in Figure 4, with LAG300um the amount of afterglow is above 0.1% of the maximum intensity even 150ms after stopping the radiation. This means in the ultra-fast scan where a tomographic acquisition can be done in less than 100ms, the residual signal from the first projection exist in all projections even in the last frame. With LAG20um and LAG100um the amount of afterglow is less than 0.1% of maximum intensity 25ms after closing the shutter. Therefore, for the applications for which the offered resolution by LAG100um is acceptable, we may prefer LAG100um to LAG20um, as LAG100um results in higher emission intensities while its afterglow is almost as small as LAG20um.

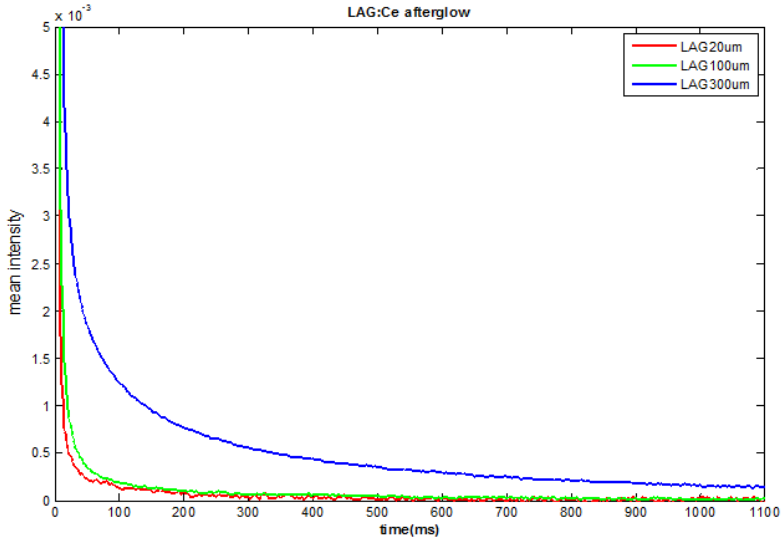

Figure 4: Afterglow of different thickness of LAG:Ce scintillator

3.2 The effect of temporal resolution (scan speed) on the afterglow artifacts

In CT scan afterglow is unfavorable especially for fast scan. Investigating the effect of acquisition rate on the afterglow artifacts, we performed several tomographic scan of the QRM-MicroCT-Barpattern (figure 5) with different exposure time and scan rate, using two different thickness of LAG scintillator, following this protocol: 10 dark frames, 400 prior flat frames, 500 projections, 400 post flat frames. More details are listed in below.

- Exposure time (for LAG:Ce 100um) : 0.1, 0.2, 0.3, 0.4, 0.5, 0.6, 0.8, 1, 3 and 5ms

- Exposure time (for LAG:Ce 300um) : 0.1, 0.2, 0.3, 0.4, 0.5, 0.6, 0.8, 1 and 2ms
- Energy: Polychromatic (white Beam with mean energy 30 keV)
- Camera: Giga-Frost, sCMOS sensor
- Microscope: 2-4x WB optics , Magnification: 2.5x, Actual pixel size : 4.4 um

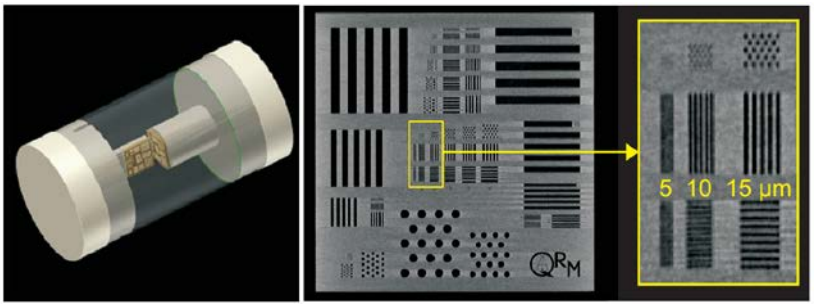

Figure 5: QRM-MicroCT-Barpattern [12]. The phantom comprises two silicon chips placed in a full resin cylinder, one orientated inplane and one perpendicular (axial) orientated to it.

All tomographic scans, reconstructed using FBP and SIRT algorithms which are implemented within the ASTRA toolbox [13], Projections and reconstructed images compared visually and quantitatively.

At first we compared the projections of different scans with different exposure time. To this end we selected one arbitrary projection (e.g. projection # 90) from 500 projections of different scans. Figure 6 shows the projection 90 of the scans with 100us, 200us, 400us and 800us exposure time. Except the projection which acquired with 100us exposure time, the bar patterns are clear in other projections and it seems that they have similar quality so it is difficult to find the effect of exposure time and afterglow artifacts from the visual comparison of projections. Table 2 compares the mean intensity of each projection which comply our expectation of higher intensity with more exposure time, but we should note that with double exposure time we do not achieve double mean intensity. This fact can be related to the charge trapping and releasing behaviour of scintillator [7, 14,15].

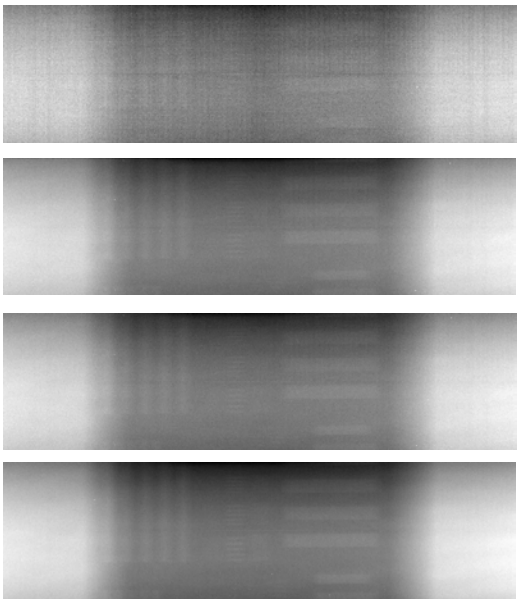

Figure 6: Projection #90 of different scans with different exposure time (from top to bottom: 100us, 200us, 400us and 800us). The contrast and brightness of the images were adjusted for better presentation

Table 2: Mean intensity of projection #90 of different scans with different exposure time

Exposure time (us)	Mean intensity
100	208
200	357
400	652
800	1258

In figure 7 we see one slice of the reconstruction results of nine scans with different amount of exposure time. Each scans contained 500 projections that acquired with the ultra-fast setup of the TOMCAT beamline and reconstructed using FBP algorithm. One projection of some of these scans has been already showed in figure 6. As it can be appreciated from the figure 6, it is hard to grasp the effect of exposure time in projections of the scans with different scan speed but in reconstruction domain some differences will be appeared which are discussed in next section. As a quantitative comparison the signal-to-noise ratio (SNR) and contrast-to-noise ratio (CNR) of the results presented in table 3. Since the TOMCAT ultrafast endstation is a continues data acquisition setup, the scan time is the multiplication of exposure time to the number of projections.

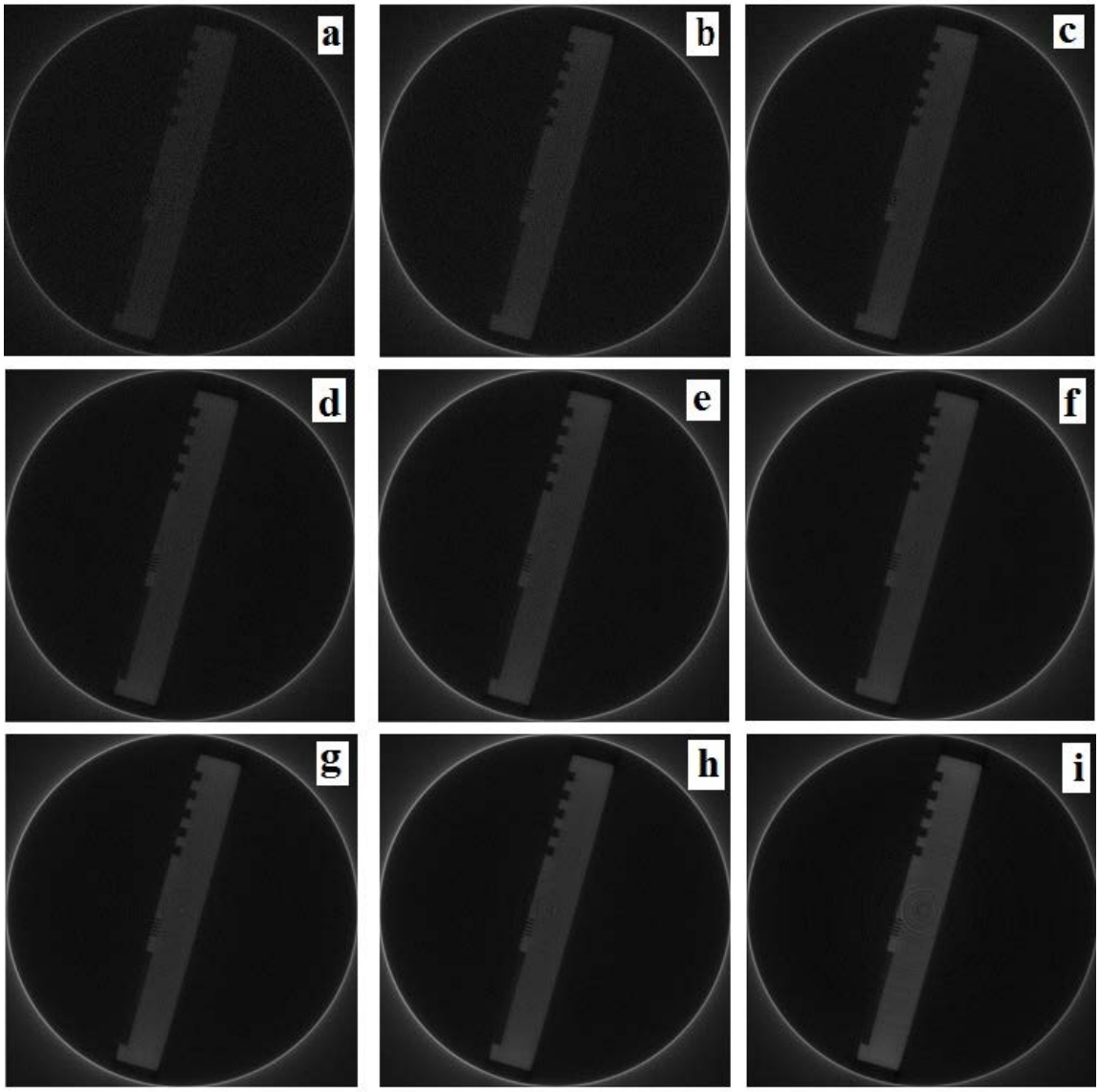

Figure 7: Reconstruction result (slice #190) of different scans with different exposure time (respectively from a to i: 100us, 200us, 300us, 400us, 500us, 600us, 800us, 1ms and 2ms). More ring artifacts appear in two last images (h and i) with the exposure time more than 1ms. The contrast and brightness of the resultant images were adjusted for better presentation.

Table 3: Quantitative comparison of reconstruction result of nine scans with different exposure time

# projection	exposure time	scan time (ms)	SNR	CNR
500	**100us**	50	0.712	0.557
500	**200us**	100	1.125	0.850
500	**300us**	150	1.448	1.088
500	**400us**	200	1.684	1.260
500	**500us**	250	1.925	1.437
500	**600us**	300	2.111	1.581
500	**800us**	400	2.435	1.836
500	**1ms**	500	2.708	2.066
500	**2ms**	1000	3.241	2.891

4. Conclusions

Afterglow is delayed luminescence from the scintillator occurring after the irradiation has stopped. This phenomenon is especially detrimental for fast X-ray imaging applications. In the present study, following the introduction and explanation of the experimental setup and methodology, we examined if the thickness of the scintillator has effect on the amount of afterglow. We demonstrated that thicker scintillators of LAG result in more afterglow but we showed that there was no significant difference between the afterglow in LAG100um and LAG20um. Therefore, considering the fact that thicker scintillators result in higher emission intensities, for the applications for which the offered resolution by LAG100um is acceptable, LAG100um may be preferred to LAG20um.

We also demonstrated the effect of exposure time on the projections and reconstructed images of different scans with different scan time. Figure 6 showed a noisy and very poor image quality in the projections of the scan with 100us exposure time, however, the reconstruction of this fastest scan amongst our experiments with a basic reconstruction algorithm such as FBP shows acceptable results for many applications in dynamic processes analysis. Therefore, thanks to the high flux at the TOMCAT beamline, even with a short exposure time (e.g. 100us) the photon counts are enough to have an object detectable reconstruction which is suitable for some dynamic processes analysis.

On the other hand, to have higher signal to noise ratio we can increase the exposure time but based on our experiments there is an optimum point for the amount of exposure time. As we can see in figure 7 more ring artifacts appear in two last images with the exposure time more than 1ms. Moreover, confirming the findings of Graham R Davis in [16], if the X-ray exposure is high, in order to achieve a high SNR, then the ring artifacts will become more dominant in relation to the random noise.

Ultra-fast endstation is a setup which is used at the TOMCAT beamline to study dynamic processes (4D) and to this end the total scan time should be as short as possible. This setup is a continues acquisition endstation and the total scan time is equal to the number of projections multiply by exposure time, consequently different combinations of these two parameters can result in same amount of scan time but probably not exactly same reconstruction results. Therefore, as a next work we plan to study how to select an optimal number of projections and exposure time.

Acknowledgments

The authors wish to express their appreciation to beamline staff for their support at the TOMCAT beamline. Rajmund Mokso is acknowledged for fruitful discussions. Networking and STSM support was provided by the EXTREMA COST Action MP1207.

References

[1] "TOMCAT Beamline." [Online]. Available: http://www.psi.ch/sls/tomcat/. [Accessed: 10-Sep-2016].

[2] Maire, Eric, et al. "*20 Hz X-ray tomography during an in situ tensile test*." International Journal of Fracture (2016): 1-10.

[3] T. M. Buzug, *Computed tomography: from photon statistics to modern cone-beam CT*. Berlin: Springer, 2008.

[4] J. Hsieh, *Computed tomography: principles, design, artifacts, and recent advances*. Bellingham, WA: SPIE Optical Engineering Press, 2003.

[5] T. Yanagida, Y. Fujimoto, T. Ito, K. Uchiyama, and K. Mori, "*Development of X-ray-induced afterglow characterization system*," Applied Physics Express, vol. 7, no. 6, p. 062401, Jun. 2014.

[6] R. Carmi, O. Shapiro, and D. Braunstein, "*Resolution enhancement of X-ray CT by spatial and temporal MLEM deconvolution correction*," Nuclear Science Symposium Conference Record, 2004 IEEE. Vol. 5. IEEE, 2004.

[7] A. Cecilia, "*Crystals for indirect and direct detectors employed in X-ray imaging applications*," Ph.D. thesis, Albert-Ludwigs-Universität Freiburg im Breisgau, 2012.

[8] J. Hsieh and King Kevin F., "*Investigation of a solid-state detector for advanced computed tomography*," IEEE Transactions on Medical Imaging, vol. 19, no. 9, pp. 930–940, Sep. 2000.

[9] S. J. Kisner, P. Jin, C. A. Bouman, K. Sauer, W. Garms, T. Gable, S. Oh, M. Merzbacher, and S. Skatter, "*Innovative data weighting for iterative reconstruction in a helical CT security baggage scanner*," pp. 1–5, 2013.

[10] http://www.crytur.cz/pages/33/crytur-materials. [Accessed: 10-Sep-2016].

[11] S. R. Stock, Microcomputed tomography methodology and applications. Boca Raton: CRC Press, 2008 , ISBN 9781420058765.

[12] http://www.qrm.de/content/products/microct/microct_barpattern.htm

[13] W. van Aarle, W J. Palenstijn, J. De Beenhouwer, T. Altantzis, S. Bals, K. J. Batenburg, and J. Sijbers, "*The ASTRA Toolbox: a platform for advanced algorithm development in electron tomography*", Ultramicroscopy, Vol. 147, p. 35–47, (2015)

[14] J. Starman: "*Lag correction in amorphous silicon flat-panel x-ray computed tomography*", PhD dissertation submitted to the department of electrical engineering of Stanford University, Dec 2010

[15] D. Zhang, M. Shi, Y .Sun, Y.Guo and C. Chang, "*Long afterglow property of Er 3+ doped Ca 2 SnO 4 phosphor*." Journal of Alloys and Compounds 667 (2016): 235-239.

[16] Graham R. Davis ; James C. Elliott; "*Aspects of x-ray microtomography equipment design"*. Proc. SPIE 5535, Developments in X-Ray Tomography IV, 182 (October 26, 2004);